Heterotypic intercellular adhesion tunes efficiency of cell-on-cell migration

Chandrashekar Kuyyamudi[1,2]*#, Suhrid Ghosh[1,2]#, & Cassandra G. Extavour[1,2,3]*

1. Department of Organismic & Organismic Biology, Harvard University. Cambridge, MA, USA
2. Howard Hughes Medical Institute. Chevy Chase, MD, USA
3. Department of Molecular & Cellular Biology, Harvard University. Cambridge, MA, USA

* Correspondence: CK ckuyyamudiashwinikumar@fas.harvard.edu

CGE extavour@oeb.harvard.edu

# These authors contributed equally.

Significance Statement

Cell adhesion is important for cell migration, and when cells migrate on a substrate of other cells (rather than on extracellular matrix), the adhesive properties of both cell types must be considered. However, whether and how dynamic changes in adhesion regulate cell-on-cell migration remains unclear. Here we approach this problem using transepithelial migration of *Drosophila* embryonic germ cells as a case study. We develop an *in silico* model of the migration process that predicts an optimal level of adhesion between migrating cell and substrate cell to achieve efficient migration. *In vivo* live imaging and genetic manipulation experiments uphold the predictions of this model. This suggests that adhesion is not a simple on/off binary parameter regulating migration.

Abstract

Cell migration across epithelial barriers occurs in diverse developmental, immunological, and pathological contexts. Here we investigate the contribution of heterotypic adhesion between migrating cells and epithelial "substrate" cells to transepithelial migration. Using an *in silico* model inspired by the migration of primordial germ cells across the midgut epithelium in the *Drosophila* embryo, we show that heterotypic adhesion modulates migration efficiency in a non-monotonic manner, revealing the existence of an optimal adhesion regime. Consistent with this prediction, *in vivo* overexpression of E-cadherin in germ cells accelerated their exit from the midgut relative to controls. Beyond providing experimentally testable predictions, our model integrates and explains previous observations on the role of heterotypic adhesion in cell-on-cell migration, offering a framework for understanding transepithelial migration across biological contexts.

Keywords:

Germ cell migration, intercellular adhesion, E-cadherin, Cellular Potts model, CompuCell3D, *in vivo* live imaging

45 **Introduction**

46 Cells frequently carry out their functions at locations distinct from their site of origin,
47 making the individual cellular motility that is required for cell migration a critical
48 aspect of their behavior (1, 2). To achieve motility, cells require persistent and directed
49 membrane activity, which is frequently guided by external chemical cues (3–6). This
50 directed membrane activity is enabled by the dynamic nature of cell membranes, which
51 exhibit continuous turnover of cytoskeletal components (7–9)

52 Cell migration, division, differentiation and death enable the development of
53 multicellular organisms from a single cell (10). Cells in various developmental contexts
54 migrate individually as well as collectively (1, 2, 11). Embryonic development unfolds
55 as a tightly regulated cascade of events, where each step must occur within a specific
56 time window to prevent disruption of subsequent stages (12–15). These temporal
57 constraints also apply to cell migration, making not only the path taken but also the
58 timing of arrival critical to proper development (1, 2, 16, 17).

59 In the developing embryo of the fruit fly *Drosophila melanogaster*, the primordial
60 germ cells (germ cells) are the first cells to form (18). The germ cells form at the
61 posterior tip of the embryo roughly 2.5 hours after egg laying (18, 19). Around 15
62 minutes after their formation, the embryo undergoes gastrulation, and the cluster of
63 germ cells enters the primordial midgut upon invagination of the surrounding tissue
64 during gastrulation (20). Here, the germ cell cluster eventually disassembles, and the
65 germ cells exit the gut by individually passing through the monolayer of epithelial cells
66 that form the midgut (20, 21). Recent work has implicated juvenile hormones as
67 chemical cues that guide germ cells toward the posteriorly located gonad (22).

68 Complementing this, Wunen/Wunen2, strongly expressed on the ventral side of the
69 midgut, acts as a repellent that drives germ cells to exit the midgut dorsally (23–26).
70 Once outside the midgut, the germ cells continue their migration to join the
71 mesodermal cells that form the somatic gonad primordium (27).

72 The *Drosophila* adhesion protein E-cadherin is encoded by the *shotgun* (*shg*) gene,
73 and is maternally deposited in the early embryo (28, 29). Germ cells require this
74 maternally deposited E-cadherin both to form a cohesive cluster and to tether to the
75 invaginating midgut primordium during gastrulation (30–32). Regulation of germ cell
76 E-cadherin during internalization into the midgut is orchestrated by the Trapped in
77 endoderm (Tre1) protein, a G protein-coupled receptor (31, 32). Tre1 enables the germ
78 cell cluster to form a radial configuration of polarized cells that detach from the cluster
79 prior to transepithelial migration (31, 32). In embryos laid by females expressing a loss
80 of function *shotgun* allele (shg^{A9-49}), individual germ cells separate from the cluster
81 prematurely (31). Furthermore, in 38% of shg^{A9-49} mutant embryos, germ cells exhibit a
82 delay in crossing the midgut epithelium (31). The posterior midgut, which is the barrier
83 that the germ cells must breach, is made up of epithelial cells (33, 34). Remodeling of the
84 midgut epithelium endows the epithelial barrier with increased permeability, allowing
85 the germ cells to migrate through it (20, 35). High resolution imaging of the germ cells
86 crossing the midgut epithelium has shown that germ cells maintain contacts with the
87 epithelial cells with no evident intercellular space around them (20). In addition, FGF
88 signaling regulates the distribution of zygotic E-cadherin in the posterior midgut to
89 maintain its epithelial integrity (36). FGF mutants display mislocalized E-cadherin and
90 collapse of the midgut lumen, trapping the germ cells within (36).

91 Germ cells expressing defective E-cadherin (shg^{A9-49}) show delayed
92 transepithelial migration (31), reminiscent of the delay in border cell migration that
93 occurs when nurse cells either lack or overexpress E-cadherin in the *D. melanogaster* egg
94 chamber (37). Together, these observations suggest the existence of a non-monotonic
95 relationship between migration efficiency and adhesion between migrating and
96 substrate cells. We set out to understand the role of heterotypic adhesion between the
97 migrating cells and "substrate" cells in transepithelial migration, taking as a case study
98 the role of intercellular adhesion mediated by E-cadherin in enabling the germ cells to
99 transmigrate. Leveraging genetic tools and two-photon microscopy, we live imaged the
100 process of transepithelial migration *in vivo.* We combined the insights gained from live
101 imaging with previously published observations to formulate an *in silico* model of the
102 process. This model, formulated in the Cellular Potts Model framework (38–40),
103 provides a novel mechanistic understanding of this transepithelial migration process.
104 Our model reveals the existence of optimal heterotypic adhesion between germ cells
105 and the epithelial cells, which maximizes the efficiency of midgut exit. In addition, our
106 *in silico* model yields testable, potentially generalizable predictions about the role of E-
107 cadherin and intercellular adhesion that may be applicable to other systems of
108 heterotypic cell adhesion and migration.

109 **Results**

110 ***I. Germ cells exit the midgut individually and maintain E-cadherin***
111 ***expression throughout exit***

112 To gain insight into the process of germ cell transepithelial migration, we live imaged
113 the process *in vivo* [**Fig. 1b-b″**]. Before migration, the germ cells are contained by the
114 epithelial barrier of the midgut [**Fig. 1b**], and located at a depth of more than 25μm from
115 the cortex within the embryo (41). To visualize the germ cells, we used the previously
116 generated fly line *nos-LifeAct-tdTomato* (42) which specifically labels germ cell
117 membrane and cortex through posteriorly localized maternally deposited protein. The
118 cells in the gut epithelium also show some residual labelling since the gut arises from
119 the invaginating posterior blastoderm. The residual labelling generates contrast and
120 helps us estimate the position of the gut during transepithelial migration.

121 We tracked germ cells throughout transepithelial migration, characterizing their
122 progress at a five minute time resolution [**SI Videos 1 - 3**], and quantified the distances
123 of germ cells from the center to the edge of the midgut lumen as a function of time [**Fig.**
124 **1 c**]. **Figure 1d-d′** shows the distance covered relative to their initial position (i.e. t = 0)
125 as a function of time for two different embryos. We found that individual germ cells
126 took 30 minutes on average to go through the midgut epithelial barrier [**Fig. 1d-d′; SI**
127 **Videos 1 - 3**]. Our live imaging of the transepithelial migration process did not reveal
128 any cell divisions in the midgut epithelial cells that could have generated spaces in the
129 epithelial barrier that would allow for easier exit of germ cells, in contrast to the
130 mechanism that regulates macrophage infiltration in *D. melanogaster* (43).

To examine E-cadherin dynamics during the transepithelial migration, we generated a fly line expressing endogenously GFP tagged Vasa and mScarlet tagged E-cadherin [**SI Methods**]. Using multi-photon confocal microscopy, we observed that E-cadherin in germ cells changed its subcellular localization at the start of the transepithelial migration [**SI Figure 5 a,a′,b, b′; SI Video 6**]. We observed E-cadherin in the epithelia also move laterally upon germ cell entry [**SI Figure 5 c,c′; SI Video 6**]. Imaging individual germ cells at higher time resolution revealed transient E-cadherin foci form at the interface of germ cell and lateral gut epithelia [**SI Figure 5 d,d′; SI Video 7**]. These foci appear to anchor the germ cell to the baso-lateral epithelial membrane as the germ cells moves forward [**SI Video 7**] and exit the gut. Our observations from live imaging were further bolstered by our ~~We also~~ observation of E-cadherin localization on the surface of germ cells during the transepithelial migration, detected by immunostaining for GFP in endogenously GFP-tagged E-cadherin embryos [**Fig. 1e-e′**]. This result is consistent with previously published experiments (31) that detected E-cadherin by immunostaining.

We quantified the intensity of E-cadherin signal at apical and lateral junctions between midgut epithelial cells, as well as at the epithelial-germ cell junctions [**Fig 1e′′**]. Our quantification revealed that the E-cadherin concentration at the germ cell-epithelial cell interface is not significantly different from that observed between epithelial cells on the lateral side ($p= 0.31$) [**Fig. 1e′′**]. The presence of E-cadherin in germ cells during transepithelial migration, where germ cells physically contact epithelial cells (20), along with the delayed midgut exit previously observed in *shg* loss of function mutants (31), suggests that the expression of E-cadherin in germ cells is functional rather than incidental.

155

156 ***II. Time to exit the midgut has a non-monotonic dependence on germ cell***
157 ***E-cadherin level***

158 Although inspired by germ cell transepithelial migration, our central question is
159 broader: what role does heterotypic E-cadherin adhesion play in cell migration? To
160 generalize our question beyond germ cell transepithelial migration, we turned to *in*
161 *silico* modeling, retaining only essential features of the phenomenon. We developed a
162 two-dimensional model of transepithelial migration, where a single motile cell breaches
163 a ring of epithelial cells under the influence of an external, radial chemoattractant
164 gradient [**Fig. 2a**]. Our two-dimensional model, formulated as a Cellular Potts Model
165 (38, 39), enabled us to consider the cells as finite sized objects capable of deformations in
166 shape. We primarily explored the potential role of chemoattractant strength (λ_M) and
167 the concentration of E-cadherin in the germ cells (C_G) in the time taken for the germ cells
168 to exit the epithelial barrier (τ_e). We ran our simulations for a maximum of 10,000
169 Monte Carlo steps, and saved the position of the germ cell as a function of time for each
170 independent iteration for a given choice of system parameters. **Figure 2a** shows a
171 typical snapshot from our CompuCell3D simulation, and **Figure 2b-b''** shows the
172 modeled germ cell at three different stages of the transepithelial migration. In the CPM
173 framework, the temperature parameter (T) controls boundary pixel activity, where
174 higher temperatures increase the likelihood of energy-raising pixel flips. To investigate
175 how membrane fluctuations at interepithelial junctions affect migration, we modulated
176 the temperature governing pixel acceptance rates at these boundaries. This allowed us
177 to study how epithelial remodeling influences transepithelial migration.

178 Our simulations [**Fig. 2c-c′**] revealed that elevated epithelial temperature
179 increased tissue permeability to germ cells, resulting in faster exit times (τ_e) and higher
180 escape probabilities (p_e). This is consistent with prior experimental findings where
181 failure in epithelial remodeling of the midgut adversely affected germ cell
182 transepithelial migration (20, 35, 44).

183 The strength of the modeled chemoattractant λ_M beyond which germ cells
184 successfully migrated through the barrier was positively correlated with epithelial cell
185 E-cadherin concentration C_E [**Fig. 3a–a′′**]. We interpret this to mean that higher C_E
186 values, indicating stronger adhesion between the epithelial cells, offered greater
187 resistance to the trans-migrating cell. Regardless of the value of C_E, we observed that
188 the time taken to exit the barrier decreased with increased germ cell E-cadherin
189 concentration only up to a point, beyond which there was a sharp increase in the time
190 taken to breach the epithelial barrier [**Fig. 3a–a′′**]. This non-monotonic dependence of τ_e
191 on C_G suggested that there is an optimal range of heterotypic adhesion between germ
192 cell and the epithelial cell. Within this range, adhesion aids the transepithelial
193 migration, but beyond the range, it hinders germ cell movement. The minima of the
194 curves for different values of λ_M in **Figure 3a–a′′** coincide, indicating that the optimal
195 adhesion value for transepithelial migration is independent of the chemoattractant
196 strength. Interestingly, the coefficient of variation in the time to exit τ_e as a function of
197 C_G has a trend that is inverse of the one exhibited by τ_e [**Fig. 3b**]. Specifically, the
198 coefficient of variation is highest when the mean is the lowest, which is not due to
199 standard deviation being independent of C_G. Instead, the standard deviation increases
200 with C_G while the mean decreases with C_G **[SI Fig. 1].**

201 To better understand the potential role of heterotypic adhesion in determining
202 the speed of exit, we focused on the trajectories of the migrating cells at different values
203 of C_G. We ran our simulations for a maximum duration of 10,000 Monte Carlo steps (45),
204 and the cells which had not exited by then were considered to have failed to exit. In
205 **Figure 3c**, the trajectories from ~1000 independent iterations are shown for $C_G = 4.89$,
206 $C_E = 10.0$ and $\lambda_M = 7000$. While there are numerous instances of the migrating cell
207 failing at early stages of the transepithelial migration, we see many instances of germ
208 cells stuck to the outer edge of the epithelial barrier and failing to complete midgut exit.
209 At low values of CG, germ cells are stuck closer to the apical side of the midgut,
210 whereas at high values germ cells get attached to the basal side, with much of their cell
211 body outside the barrier [**SI Figure 2**]. We considered all the successful trajectories for
212 $C_E = 10$ and $\lambda_M = 7000$ and normalized the time for each trajectory, such that $\tau = 0$ and
213 $\tau = 1$ mark the start and end of the transepithelial migration respectively. The time-
214 normalized mean trajectories are shown in **Figure 3d**, colored according to their values
215 of C_G. We observed that germ cells with lower E-cadherin concentrations spent much of
216 their time getting to the middle of the epithelial barrier, while the second half of the
217 journey, culminating in complete exit from the midgut, was quite rapid. The fraction of
218 total time spent in getting to the middle dropped with increasing germ cell–epithelial
219 cell adhesion, with speed through the barrier becoming constant for high values of C_G
220 (~7.0). To highlight the difference in the fraction of total travel time spent at different
221 halves of the epithelial barrier, we show the fraction of time spent to cover the second
222 half of the epithelial barrier (referred to as τ_2) in **Figure 3d'**. τ_2 showed a nonlinear
223 increase with C_G approaching 0.5 at lager values of C_G. The probability of success in
224 exiting the epithelial barrier had an inverse non-linear relation to time to exit τ_e

225 regardless of the C_E, C_G and λ_M, as evident from the scatter plot in **Figure 3e**. The model
226 also predicts that there is an optimal concentration of E-cadherin in the substrate [**SI**
227 **Figure 4**], consistent with the hypothesis that the efficiency of transepithelial migration
228 is a function of the heterotypic adhesive interface, rather than of the migrating germ
229 cells alone.

230 In accordance with previous genetic studies (25, 46, 47), we hypothesized that
231 Wunen/Wunen2, which is strongly expressed ventrally, repels germ cells and biases
232 their exit toward the dorsal side. When we incorporated a dorsoventral chemical
233 gradient alongside the radial gradient, germ cells exited the epithelial barrier more
234 dorsally, supporting this hypothesis [**SI Figure 3**].

235 *III. Overexpression of E-cadherin in germ cells leads to faster exit through*
236 *the midgut*

237 The results of our model suggested that increasing E-cadherin levels in germ cells
238 would enable them to complete the most time-consuming part of their journey, namely
239 traversing from the middle of the midgut lumen through the luminal epithelial surface,
240 more rapidly, thus resulting in a faster net transepithelial migration time. To test this
241 prediction *in vivo*, we employed the UAS-GAL4 system (48). Maternally deposited E-
242 cadherin serves as the primary source of E-cadherin for all early embryonic cells,
243 including both germ cells and somatic cells (29, 31, 49). Notably, even during
244 transepithelial migration (~3 hours after egg laying), germ cell E-cadherin remains
245 predominantly of maternal origin, making RNAi-mediated knockdown in germ cells
246 impractical without destroying embryonic integrity (29, 31, 49).

247 Given these constraints, to assess the effects of E-cadherin overexpression on
248 transepithelial migration, we analyzed germ cell progression in embryos of four
249 different maternal genotypes, collected within 30 minutes from synchronously
250 ovipositing mothers and aged for five hours, as follows: (I) **WT**: Outcrossed wild-type
251 control, expressing endogenous levels of E-cadherin in all cells [*nos-Gal4/+*]; (II) **Pan-**
252 **Ecad-OE-A**: with ubiquitous E-cadherin overexpression in all cells [*nos>Ecad*]; (III) **Pan-**
253 **Ecad-OE-B**: with ubiquitous GFP-tagged E-cadherin overexpression in all cells
254 [*nos>Ecad-GFP*]; and (IV) **GC-Ecad-OE**: with germ cell-targeted overexpression of
255 mClover2-tagged E-cadherin [*nos> Ecad-mClover2-nosTCE-pgc 3'UTR*]. To assess the
256 extent of overexpression achieved, we quantified germ cell E-cadherin relative to
257 epithelial apical and lateral expression using anti-DE-cadherin immunostaining [**SI**
258 **Figure 7**]. The results of this quantification confirmed that use of the ubiquitous driver
259 increased E-cadherin levels in both germ cells and the somatic epithelium, and that the
260 germ cell driver increased E-cadherin levels in germ cells but not somatic cells [**SI**
261 **Figure 7**]. The position of germ cells relative to the midgut lumen boundary in
262 representative embryos from each group is shown in **Figure 4a–a'''**. Quantitative
263 analysis revealed that germ cells in all overexpression lines (II–IV) were located farther
264 from the lumen center compared to controls (I) [**Fig. 4b**]. Furthermore, both the mean
265 germ cell distance from the lumen center [**Fig. 4c**] and the fraction of germ cells that had
266 exited the midgut [f_{exit} in **Fig. 4d**] were higher in overexpression groups, with the most
267 pronounced effect in the germ cell-targeted overexpression line (IV).

268 These results suggest that higher levels of E-cadherin in germ cells accelerates
269 transepithelial migration, consistent with our theoretical model. We favor the
270 interpretation that wild-type germ cell E-cadherin expression is associated with an

271 intermediate time to exit [gray bar, **Fig. 4e**]. Under this interpretation, loss of function
272 *shg* mutants like shg^{49-49} (31) would drive the embryo toward the red region shown in
273 **Figure 4e**, associated with longer τ_e, while *shg* overexpression would drive it towards
274 the green region in **Figure 4e** associated with faster germ cell exit.

275 Our model predicted that elevated epithelial E-cadherin would hinder migration
276 by increasing resistance to germ cell exit. Germ cells in our experiments overexpressing
277 E-cadherin in both somatic and germ cells showed reduced germ cell exit times. This
278 apparent discrepancy can be explained by the hypothesis that wild-type E-cadherin
279 levels in somatic epithelial cells are already near saturation. Under this interpretation,
280 finite adhesion junction availability and membrane transport limitations would prevent
281 additional E-cadherin from forming new junctions at high concentrations (50–53). Thus,
282 in embryos with E-cadherin overexpression in both germ cells and somatic cells, like the
283 ones we examined herein (**Fig. 4,** groups II and III), we hypothesize that E-cadherin
284 levels higher than wild type levels would have a stronger effect on germ cells than on
285 epithelial cells, effectively mimicking germ cell-specific overexpression.

286 To further test this, we drove zygotic expression of GFP-tagged E-cadherin
287 specifically in the gut using the 48Y-GAL4 endodermal driver (54) [**SI Figure 6a, b**]. We
288 observed only a small, statistically insignificant decrease in the fraction of germ cells
289 that had exited the gut relative to controls [**SI Figure 6f**]. Because the 48Y-GAL4 driver
290 drives detectable expression 30 minutes after transepithelial migration has initiated [**SI**
291 **Figure 6b**], it could be the case that our experiment changed E-cadherin levels too late
292 to severely perturb the process. However, this result suggests that overexpression of E-
293 cadherin in the already E-cadherin-rich epithelium has little effect on transepithelial
294 migration, in contrast to germ cell-specific overexpression.

295 We next used the 48Y-GAL4 driver to induce gut-specific knockdown of E-
296 cadherin (shg-RNAi) and observed a statistically significant reduction in the fraction of
297 germ cells exiting the midgut compared to wild type controls [**SI Figure 6f**]. This
298 phenotype mirrors what Parés and Ricardo (36) reported for FGF pathway mutants,
299 where mislocalization of epithelial E-cadherin caused a substantial proportion of germ
300 cells to fail to exit the midgut. These observations are consistent with our hypothesis
301 that epithelial E-cadherin, and not just germ cell E-cadherin, is required for successful
302 germ cell transmigration. We note that we cannot rule out the alternative hypothesis
303 that germ cell transepithelial migration is impeded in this condition because of broad
304 defects in gut architecture that might be present since epithelial E-cadherin is integral to
305 the structural integrity of the gut and its lumen (36). However, if the gut epithelium
306 were indeed weaker because of E-cadherin depletion, we would expect more efficient
307 germ cell exit, which is the opposite of what we observed. We therefore favor the
308 hypothesis that E-cadherin expression in the gut epithelium is an important contributor
309 to the heterotypic interactions that are required for germ cell exit from the gut.

310 Discussion

311 Our work sheds light on the potential role of heterotypic E-cadherin adhesion during
312 the transepithelial migration of germ cells through the midgut. Further, the predictions
313 of our *in silico* model could in principle apply to any heterotypic adhesive migration
314 process, as we incorporated only a few features specific to germ cell transepithelial
315 migration. Our model logic consists of three key elements, i) a migrating cell that forms
316 transient heterotypic adhesive contacts with a barrier epithelium/endothelium, ii) a
317 chemoattractant gradient providing directed motility, and iii) an optimal adhesion
318 range, where too little adhesion fails to provide the traction needed to breach the

319 barrier, while too much adhesion impedes forward movement by making junction
320 disassembly rate-limiting. We believe this logic is general, while the migratory and
321 substrate cell type, the molecular identity of the adhesion molecules and the source of
322 the driving force are specific to the system.

323 Our results suggest a non-monotonic dependence of migration efficiency on the
324 heterotypic adhesion between the migrating cell and the substrate cells [**Fig. 4d**]. We
325 posit that traction is essential for cell migration, and that transmembrane proteins like
326 integrins facilitate traction by anchoring cells to the extracellular matrix, thereby
327 enabling forward movement (55). Additionally, cadherin-like molecules mediate
328 homotypic adhesion, allowing cells of the same type to form cohesive tissues such as
329 epithelia (49, 56). These molecules also participate in heterotypic adhesion when
330 migrating cells interact with others expressing cadherins (57–59). A notable example is
331 the transendothelial migration of melanoma cells, where heterotypic adhesion is clearly
332 observed (57). Melanoma cells form heterotypic N-cadherin mediated adhesion
333 junctions with the endothelial cells during their migration (57, 60). Based on our model,
334 we predict a non-monotonic relationship between transmigration efficiency and the
335 heterotypic adhesion between melanoma cells and endothelial cells. More broadly,
336 diapedesis - the process by which cells breach endothelial barriers - relies on heterotypic
337 interactions between transmembrane adhesion proteins (58, 59). The prevalence of
338 heterotypic adhesion during transepithelial migration suggests that our work may have
339 broader implications beyond the specific context of *Drosophila* primordial germ cell
340 migration.

341 Many conserved features of cell migration are applicable well beyond a specific
342 biological context. In a migrating cell, actin filaments polymerize at the leading edge

343 and undergo retrograde flow, functioning much like the rotation of wheels in a car (61–
344 63). However, the forward motion of a cell depends on its physical coupling to the
345 substrate, just as the tires of a car grip the road to provide traction (61, 62, 64). This
346 mechanism is described by the *molecular clutch model* of cell motility (65). Adhesion
347 molecules such as integrins and cadherins allow cells to bind to surfaces or to other
348 cells, engaging the molecular clutch (65, 66). Integrin-mediated traction is typically used
349 when cells migrate over an extracellular matrix, whereas cadherins facilitate cell-on-cell
350 migration, as seen in the case of border cell migration (37, 66), and in the transepithelial
351 migration case that we consider here.

352 Our *in silico* model predicts that an intermediate adhesion strength between
353 migrating cells and substrate cells optimizes transmigration. Our finding aligns with
354 previous observations on *D. melanogaster* border cell migration in the egg chamber (37,
355 67). In the case of border cell migration, a cluster of six to eight border cells, enclosing a
356 pair of non-motile polar cells, migrates through a "substrate" formed by nurse cells (67).
357 Of these three cell types, polar cells express the highest levels of E-cadherin, which they
358 use to anchor to motile border cells, which have the second highest E-cadherin levels
359 (37). Meanwhile, border cells form transient junctions with nurse cell E-cadherin (which
360 is at the lowest levels of the three cell types in the system), pulling on nurse cells as they
361 migrate (37). Notably, E-cadherin knockdown in nurse cells impedes migration more
362 severely than knockdown in border cells, whereas E-cadherin overexpression in nurse
363 cells slows migration (37). These observations further support the concept that
364 intermediate heterotypic adhesion is optimal for transmigration, specifically E-cadherin
365 enabling the engagement of a molecular clutch (66).

366 Since the Cellular Potts model framework is rooted in Steinberg's differential
367 adhesion hypothesis (38, 39, 68), transepithelial migration can be interpreted through
368 this lens. In this framework, epithelial cells, by virtue of their high E-cadherin
369 expression, strongly prefer to bind one another, creating a thermodynamic barrier that
370 the germ cells need to breach to intercalate into the epithelium. Germ cell expression of
371 E-cadherin allows them to compete directly with these homotypic epithelial junctions.
372 While germ cells form fewer adhesive contacts than two epithelial cells can form with
373 each other, their E-cadherin expression is sufficient to make heterotypic binding
374 energetically accessible. The chemotactic gradient then provides the directional bias that
375 tips the overall energy balance in favor of heterotypic adhesion. Migration in the
376 absence of sufficient intercellular adhesion resembles climbing a slippery ladder—
377 lacking the traction needed for upward movement. Conversely, excessive adhesion is
378 akin to ascending a ladder coated in glue, where detachment becomes the limiting
379 factor. Thus, an optimal level of "stickiness" is crucial for efficient migration. Inherited
380 maternal content is known to influence germ cells' ability to migrate successfully to the
381 gonad (26). A component of this maternal content is the E-cadherin used during
382 transepithelial migration is one component of this maternally supplied content. We
383 speculate that the level of E-cadherin in each germ cell may contribute to germ cell
384 fitness during their journey to the gonad.

385 **Methods**

386 ***Fly stocks and maintenance***

387 We generated an endogenous C-terminal *shotgun*–mScarlet (referred to as E-cadherin-
388 mScarlet) fusion using scarless CRISPR/Cas9-mediated homology-directed repair in
389 *Drosophila melanogaster* (69), using homology arms flanking the *shotgun* stop codon. We
390 identified HDR events by 3xP3-DsRed fluorescence and validated correct targeting by
391 PCR [**Supporting Methods**]. Fly lines *w[1118]; P{w[+mC]=GAL4::VP16-*
392 *nanos.UTR}CG6325[MVD1]* (abbreviated herein as *nanos-gal4-VP16*; stock #4937),
393 *w[1118]; P{w[+mC]=UASp-shg.GFP}5B* (#58445), *y[1] w[*]; TI{TI}shg[GFP]* (#60584), and
394 *w[*]; P{w[+mC]=UASp-shg.R}5* (#58494) were obtained from the Bloomington
395 Drosophila Stock Center (Indiana, U.S.A.). Fly line *w[*]; TI{TI}vas*$^{EGFP.KI}$ (Vasa-GFP; stock
396 #118616;) was obtained from the Kyoto Stock Center (Kyoto, Japan). Fly lines *w; nos-*
397 *Lifeact-tdTomato-P2A-tdKatushka2-CAAX (Lifeact-tdTomato* landing site VK00027;
398 abbreviated herein as *nos-LifeAct-tdTomato*) and *w; UASp-DE-cadherin-mClover2-nosTCE-*
399 *pgc 3'UTR* (landing site attP2) *(Lin et al., 2022)* were a gift from Ruth Lehmann
400 (Whitehead Institute, MIT, USA). All flies and crosses were maintained on standard fly
401 medium (0.8% agar, 2.75% yeast, 5.2% cornmeal, 11% dextrose) in an incubator at 25˚C,
402 65% RH and 12H:12H light-dark cycle.

403

404 ***Fly crosses and embryo staging***

405 To generate over-expression of E-cadherin during transepithelial migration, UASp
406 (over-expression) or Oregon R (wild type control) lines were crossed to *nanos-gal4-VP16*
407 and heterozygous F1 virgin females were collected. 40-50 F1 virgin females were then

408 crossed with 8-10 Oregon R males and transferred into an egg collection cage with a
409 5mm apple juice agar plate as base (70). The *nanos-gal4-VP16* line is highly expressed in
410 the maternal germ line and deposited in the embryo but is not zygotically expressed in
411 the germ cells or somatic cells during TEM. In the case of *nos-LifeAct-tdTomato* and *Vasa-*
412 *GFP, E-cadherin-mScarlet* flies, an approximate 1:1 ratio of homozygous males and
413 females were transferred into an identical cage setup. Egg laying was allowed to
414 proceed in 30-minute windows and embryos were aged for five hours after the
415 midpoint of the egg laying window. After collection, embryos were either fixed
416 (embryonic over-expression) or used for live imaging (*nos-LifeAct-tdTomato* and *Vasa-*
417 *GFP, E-cadherin-mScarlet)*.

418

419 ***Live imaging***

420 Appropriately staged embryos were manually dechorionated with forceps on double-
421 sided scotch tape and attached to a standard 90 mm polystyrene Petri dish using
422 heptane glue. The dish was then filled with sterile distilled water and mounted on a
423 Zeiss LSM 980 multi-photon microscope. Using a 20x water immersion objective, the
424 total volume of the embryonic gut was imaged at a two-photon excitation wavelength
425 of 1000nm (*nos-LifeAct-tdTomato)*, and 900nm/1050nm (*Vasa-GFP, E-cadherin-mScarlet*),
426 every 1, 5 or 10 minutes for the indicated period.

427

428 ***Fixation and immunostaining***

429 Appropriately staged embryos were collected on a mesh, rinsed with Milli-Q water, and
430 dechorionated using 70%(v/v) commercial bleach until most of the embryos had lost
431 the chorion (confirmed visually). Embryos were fixed in a 1:1 mix of heptane and 4%
432 paraformaldehyde in 1X phosphate buffered saline (1X PBS) at room temperature with
433 nutation for 20 minutes. After removing the aqueous layer, an equal volume of 100%
434 methanol was added, and embryos were devitellinized by vigorous manual shaking for
435 2–3 minutes. Fixed embryos were stored in 100% methanol at –20 °C.

436 For staining, embryos were rehydrated in 1X PBS, then washed, permeabilized
437 and blocked twice for 15 minutes in PBTB (1X PBS, 0.2% Triton X-100, 1 mg/mL bovine
438 serum albumin (Sigma-Aldrich, A9418). Embryos were then incubated with primary
439 antibodies diluted in PBTB overnight at 4 °C. The next day, embryos were washed (4 ×
440 15 min, PBTB) and incubated overnight at 4 °C with fluorophore-conjugated secondary
441 antibodies and DAPI diluted in PBTB containing 4% normal goat serum (Jackson
442 Immunoresearch, 005-000-121). On the third day, embryos were washed (4 × 15 min in
443 1X PBS) and mounted in Vectashield (Vector laboratories, H1000) for imaging. Primary
444 antibodies used were rat anti-E-cadherin (1:20; DSHB, DCAD2), chicken anti-Vasa
445 (1:800) (Repouliou et al., 2025) and rabbit anti-GFP conjugated to AlexaFluor 488
446 (1:1000; Invitrogen, A-21311). Secondary antibody used was goat anti-rat (1:200)
447 conjugated to AlexaFluor 633 (Invitrogen, A-21094), goat anti-chicken (1:200)
448 conjugated to AlexaFluor 568 (Invitrogen, A-11041). DNA was stained with DAPI
449 (Sigma-Aldrich, D9542) at 1:2000 dilution of a 10 mg/mL stock.

450

451 ***Image Analysis and Quantification***

452 Live cell tracking was performed using the built-in Mastodon plugin in Fiji/ImageJ (71).
453 Cell position relative to the gut lumen was determined manually for each time point.
454 Fluorescence intensities were quantified by drawing manual regions of interest and
455 measuring mean gray values using basic tools in Fiji/ImageJ (71). Germ cell positions,
456 gut lumen boundary, and the center of the lumen were marked using the built-in Cell
457 Counter function in Fiji/ImageJ (71). Germ cells were classified as "Out" if their
458 distance from the lumen center exceeded that of the lumen boundary; otherwise, they
459 were classified as "In".

460

461 ***In silico model of transepithelial migration***

462 A cross-sectional slice of the epithelial midgut was modelled as a two-dimensional ring
463 formed by 20 epithelial cells. The epithelial ring is embedded in a radial chemical field
464 representing the spatial concentration of the chemoattractant. The magnitude of the
465 chemical concentration increases linearly with the radius, and the minimum coincides
466 with the center of the epithelial ring. At t=0, the germ cell begins slightly off-center,
467 with its initial angle randomly chosen between 0 and 360 degrees, and then migrates
468 outward toward regions of higher chemoattractant concentration.

469 Our two-dimensional model of the epithelial ring and the germ cells was
470 formulated in the Cellular Potts Model (CPM) framework (38–40). The cells in a CPM
471 are represented as a contiguous collection of pixels. Pairwise interactions between
472 pixels at the cell boundaries have an associated energy cost, J. Given two pixels a and b,
473 we use the value of $J_{a,b}$ to reflect the adhesion energy of the cells to which the two
474 interacting boundary pixels belong. Our model assumes that adhesion energy increases

475 with the number of adherens junctions formed, and that the number of adherens
476 junctions is in turn a function of the E-cadherin concentration. The maximum possible
477 number of junctions between two cells is thus determined by the surface E-cadherin
478 concentration of the cell that has fewer such molecules. As a result of our assumptions,
479 if $\sigma(a)$, $\sigma(b)$ are the indices of the cells to which pixels a and b belong, and $C(\sigma(a))$ and
480 $C(\sigma(b))$ are the E-cadherin concentrations of the two cells, then the interaction energy
481 term is $J_{a,b} = min(C(\sigma(a)), C(\sigma(b)))$. In our work, we have assumed that all epithelial
482 cells have E-cadherin concentration equal to C_E, and that all germ cells have E-cadherin
483 concentration equal to C_G. The energy function of the system of pixels is given by the
484 following equation:

485 $$\mathrm{E} = -\sum_{a,b} min(C(\sigma(a)), C(\sigma(b))) - \sum_{\sigma} \lambda_A \, (A_\sigma - A_0)^2 - \sum_{\sigma} \lambda_L \, (L_\sigma - L_0)^2$$

486 The λ_A and λ_L terms determine the magnitude of the energy cost required for a cell area
487 and perimeter to deviate from the steady state values A_0 and L_0 respectively. The
488 system is simulated using the metropolis algorithm (45), where the probability of a pixel
489 flip is related to the change in the magnitude of the energy of the system as a result of
490 that specific pixel flip. Under appropriate energy conditions, pixels at the boundary
491 may flip to the cell state of one of their neighbors that has a different cell state. At each
492 iteration of the simulation algorithm, one such potential pixel flip is considered, and the
493 pixel is flipped if the resulting system has lower energy than the current state. If the
494 pixel flip would not reduce the energy of the system, the pixel flips with probability
495 $p_{flip} = exp(-\Delta E/T)$, where ΔE is the change in energy due to the pixel flip and T is the
496 temperature. The temperature term T represents the extent of stochasticity (noise) in the

497 pixel dynamics, with higher T increasing the probability of pixel flips that increase the
498 energy of the system. Chemotaxis is implemented within the CPM framework by
499 biasing pixel flips that aid cell movement in the direction of the gradient of
500 chemoattractant. In the presence of the attractant whose value at any pixel in 2D space
501 is $M_{a,b}$, the change in energy due to a pixel flip, where a pixel at (a, b) is copying the
502 state of a pixel at (a', b') becomes $\Delta E' = \Delta E - \lambda_C\left(M_{a',b'} - M_{a,b}\right)$ (40). This additional term
503 favors the pixel flip when the chemical field value at (a', b') is higher than (a, b). To
504 prevent the epithelial ring from collapsing and forming a cell aggregate without a
505 lumen, we model the lumen as one large cell with a volume constraint. In addition, we
506 mechanically couple the epithelial cells by connecting the centroids of the adjacent cells
507 with springs using the FocalPointPlasticity plugin of CompuCell3D (72). The key
508 parameters that we explored in our work are C_G, C_E and λ_M. The CompuCell3D
509 implementation of our model can be found at
510 https://github.com/boyonpointe/GermCellTransepithelialMigration with commit ID
511 7ce2534.

512

513

514 **Acknowledgements**

515 We thank members of the Extavour Lab for helpful discussions, in particular Dr. Emily
516 Rivard and Dr. Petra Kovacikova for their comments on the manuscript. We thank Prof.
517 James Glazier for helpful discussions regarding CompuCell3D, the Drosophila
518 Genomics Research Center (NIH Grant 2P40OD010949) and Dr. Xiaona Tang for their

help in making the E-cadherin-mScarlet CRISPR flies. We thank Ruth Lehmann for sharing fly lines.

Data Availability

Scripts for Compucell3D simulations and image analysis are available at https://github.com/boyonpointe/GermCellTransepithelialMigration with commit ID 7ce2534.

Author Contributions

CK conceived of the study, designed and performed all computational experiments, performed data analysis and interpretation, and wrote the first draft of the manuscript. SG conceived of the study, designed and performed wet lab experiments, and reviewed and edited the manuscript. CGE obtained funding for the study, supervised its execution, and reviewed and edited the manuscript.

Funding

This study was supported by a postdoctoral fellowship to CK through the NSF-Simons Center for Mathematical and Statistical Analysis of Biology at Harvard (award number DMS-1764269), the Harvard Quantitative Biology Initiative, and by funds from Harvard University and the Howard Hughes Medical Institute (HHMI). CGE is an HHMI Investigator.

Conflicts of Interest

The authors declare no conflicts of interest.

543 ## Figure Legends

544

545 **Figure 1: Germ cells exit the midgut individually at comparable speeds. (a-a'')** Schematic of
546 *D. melanogaster* embryonic germ line development. The primordial germ cells are formed at the
547 posterior tip at stage 5. Following gastrulation, they are contained in the midgut at stage 7, and
548 eventually exit the midgut through transepithelial migration at stage 10. **(a''')** Schematic
549 showing the three different types of intercellular junction where we quantified E-cadherin
550 intensity. **(b-b'')** Three snapshots from live imaging of the TEM process as the germ cells make
551 their way through the midgut. **(c)** The distribution of the distances of the germ cells from
552 center of the midgut lumen at five different time points are shown. Small numbers under plots
553 indicate sample sizes (number of cells). **(d- d'')** Movement of germ cells in time measured with
554 respect to their initial (t = 0) position for two different live imaged embryos. Black circles:
555 positions within lumen; magenta rhomboids: positions within the midgut epithelium; white
556 squares: positions outside the midgut. **(e)** Higher magnification of the midgut during germ cell
557 transepithelial migration. Magenta: E-cadherin; green: germ cell-specific protein Vasa. **(e')**
558 Germ cells express E-cadherin during the transepithelial migration (boxes). **(e'')** The relative
559 intensity (au: arbitrary units) of the E-cadherin fluorescent signal at the epithelial cell – germ
560 cell junction (EG), lateral epithelial – epithelial junction (E_{lat}) and apical epithelial – epithelial
561 junctions (E_{api}). n = 24 junctions for each of the three categories. Two-sample Mann-Whitney
562 U tests were used to compute the p values that are shown in panel (e'') for pairwise
563 comparisons of distributions.

564

565 **Figure 2: Greater epithelial junctional remodeling aids germ cell transmigration.** (**a)**
566 Snapshot of Cellular Potts Model simulation of a germ cell (yellow) exiting the two-
567 dimensional epithelial ring (green). Pixels at the boundary of the cells are shown in black.
568 Colored arrows point in the direction of chemoattractant gradient; colors represent the
569 concentration of the chemoattractant. **(b-b'')** Snapshots of the germ cell (b) before entering the
570 epithelial barrier, (b') while inside the barrier and (b'') just before exiting the barrier. Numbers
571 at top right indicate the time in units of Monte Carlo steps (mcs). **(c)** Average time taken (τ_e)
572 for the germ cell to exit the midgut decreases with increase in interepithelial dynamics (T_E).
573 **(c')** Probability of successfully exiting (p_e) increases with T_E. Trends in c and c' are
574 independent of the strength of the chemoattractant (λ_M). The shaded silver line corresponds to

575 $T_E = 10$, the value at which al simulations described herein are carried out, unless specified
576 otherwise. Simulation parameters: $\lambda_M = 7000, C_E = 10, C_G = 5, T = 10$.

577

578 **Figure 3: Time to exit the epithelial barrier has a non-monotonic dependence on germ cell E-**
579 **cadherin concentration. (a-a'')** The time a simulated germ cell takes to exit the 2D midgut
580 epithelial barrier as a function of germ cell E-cadherin concentration (C_G). (a), (a') and (a'')
581 represent increasing epithelial cell E-cadherin concentrations ($C_E = 8$, $C_E = 10$, $C_E = 12$
582 respectively), offering increasing resistance to the germ cell transepithelial migration. The
583 curves in each of the three panels are colored according to the strength of the chemical field
584 (λ_M). Regardless of the value of C_E, for strong enough values of λ_M the time to exit shows a
585 minimum that is independent of the λ_M value. X-axis label "C_G" underneath **(a'')** applies also to
586 **(a)** and **(a')**. **(b)** The coefficient of variation in time to exit as a function of C_G for the case of $C_E =$
587 10. **(c)** Trajectories of germ cells for a typical parameter set obtained from 1000 independent
588 stochastic simulations. Silver: successful TEM; brown: germ cell exit failure; black lines: mean
589 position of the epithelial cells forming the 2D barrier. **(d)** Mean distance covered by the germ
590 cell within the barrier (l_e) as a function of time . The time τ is normalized by the total time of
591 travel, where 0 represents time of entry into the barrier and 1 represents time of exit. When the
592 germ cell E-cadherin concentration is low, the germ cell covers much of the distance in a very
593 short interval of time at the end of the journey. Higher germ cell E-cadherin levels lead to the
594 germ cell migrating at roughly uniform speed throughout the journey. **(d')** The time taken to
595 cover the second half of the journey τ_2 as a function of germ cell E-cadherin concentration. **(e)**
596 The relationship between τ_{exit} and p_{exit} is shown using data aggregated by simulating the
597 model over various values of λ_M, C_G and C_E. τ_{exit} decreases monotonically with p_{exit}, implying
598 that the shorter the time to exit, the higher the chances of exiting.

599

600 **Figure 4: Higher germ cell E-cadherin promotes quicker midgut exit *in vivo*. (a)** (L-R)
601 Representative micrographs showing the extent of transepithelial migration in the four
602 experimental groups. I corresponds to the control, II and III represent lines where E-cadherin
603 is overexpressed in all cells and IV corresponds to embryos where E-cadherin overexpression
604 is targeted to the germ cells. **(b)** The distribution of distances of germ cells from the center of

605 the lumen for the four experimental groups. Gray and black symbols represent cells inside and
606 outside the gut respectively. The distances of the germ cells from the lumen are largest in the
607 condition with increased germ cell-targeted E-cadherin overexpression (IV). Small numbers
608 under plots indicate sample sizes (number of germ cells). **(c)** Mean distance of the germ cells
609 from the center of the lumen in each embryo for the four experimental groups. Small numbers
610 under plots indicate sample sizes (number of embryos). **(d)** Fractions of germ cells per embryo
611 that have exited the midgut by 5.25 hours after egg laying in the four experimental groups.
612 Small numbers under plots indicate sample sizes (number of embryos). Two sample Mann-
613 Whitney U test was used to compute the p values that are shown in panels **(b)-(d)** for pairwise
614 distribution comparisons. **(e)** We hypothesize that the WT embryos (group I) have C_G in the
615 pink shaded region, and that germ cell-targeted E-cadherin expression pushes the system
616 towards the green shaded region, leading to shortening of τ_e.

617

618 **References**

619

620 1. A. Aman, T. Piotrowski, Cell migration during morphogenesis. *Dev. Biol.* **341**, 20–33 (2010).

621 2. E. Scarpa, R. Mayor, Collective cell migration in development. *J. Cell Biol.* **212**, 143–155
622 (2016).

623 3. D. Dormann, C. J. Weijer, Chemotactic cell movement during development. *Curr. Opin.*
624 *Genet. Dev.* **13**, 358–364 (2003).

625 4. P. Roca-Cusachs, R. Sunyer, X. Trepat, Mechanical guidance of cell migration: lessons from
626 chemotaxis. *Curr. Opin. Cell Biol.* **25**, 543–549 (2013).

627 5. E. T. Roussos, J. S. Condeelis, A. Patsialou, Chemotaxis in cancer. *Nat. Rev. Cancer* **11**, 573–
628 587 (2011).

629 6. S. SenGupta, C. A. Parent, J. E. Bear, The principles of directed cell migration. *Nat. Rev. Mol.*
630 *Cell Biol.* **22**, 529–547 (2021).

631 7. M. Bezanilla, A. S. Gladfelter, D. R. Kovar, W.-L. Lee, Cytoskeletal dynamics: A view from
632 the membrane. *J. Cell Biol.* **209**, 329–337 (2015).

633 8. K. Rottner, T. E. B. Stradal, Actin dynamics and turnover in cell motility. *Curr. Opin. Cell*
634 *Biol.* **23**, 569–578 (2011).

635 9. S. Seetharaman, S. Etienne-Manneville, Cytoskeletal Crosstalk in Cell Migration. *Trends Cell*
636 *Biol.* **30**, 720–735 (2020).

637 10. S. F. Gilbert, S. F. Gilbert, *Developmental Biology*, 6th Ed. (Sinauer Associates, 2000).

638 11. P. Friedl, D. Gilmour, Collective cell migration in morphogenesis, regeneration and cancer.
639 *Nat. Rev. Mol. Cell Biol.* **10**, 445–457 (2009).

640 12. W. T. Boyce, M. B. Sokolowski, G. E. Robinson, Genes and environments, development and
641 time. *Proc. Natl. Acad. Sci.* **117**, 23235–23241 (2020).

642 13. M. Ebisuya, J. Briscoe, What does time mean in development? *Development* **145**, dev164368
643 (2018).

644 14. A. Kicheva, M. Cohen, J. Briscoe, Developmental Pattern Formation: Insights from Physics
645 and Biology. *Science* **338**, 210–212 (2012).

646 15. J. Negrete, A. C. Oates, Towards a physical understanding of developmental patterning.
647 *Nat. Rev. Genet.* **22**, 518–531 (2021).

648 16. C. M. Franz, G. E. Jones, A. J. Ridley, Cell Migration in Development and Disease. *Dev. Cell*
649 **2**, 153–158 (2002).

650 17. C. J. Weijer, Collective cell migration in development. *J. Cell Sci.* **122**, 3215–3223 (2009).

651 18. A. F. Huettner, The origin of the germ cells in Drosophila melanogaster. *J. Morphol.* **37**, 385–
652 423 (1923).

653 19. M. Rabinowitz, Studies on the cytology and early embryology of the egg of Drosophila
654 melanogaster. *J. Morphol.* **69**, 1–49 (1941).

655 20. M. K. Jaglarz, K. R. Howard, The active migration of Drosophila primordial germ cells.
656 *Development* **121**, 3495–3503 (1995).

657 21. A. C. Santos, R. Lehmann, Germ Cell Specification and Migration in Drosophila and
658 beyond. *Curr. Biol.* **14**, R578–R589 (2004).

659 22. L. J. Barton, *et al.*, Juvenile hormones direct primordial germ cell migration to the
660 embryonic gonad. *Curr. Biol.* **34**, 505-518.e6 (2024).

661 23. K. Hanyu-Nakamura, S. Kobayashi, A. Nakamura, Germ cell-autonomous Wunen2 is
662 required for germline development in Drosophila embryos. *Development* **131**, 4545–4553 (2004).

663 24. A. D. Renault, Y. J. Sigal, A. J. Morris, R. Lehmann, Soma-Germ Line Competition for Lipid
664 Phosphate Uptake Regulates Germ Cell Migration and Survival. *Science* **305**, 1963–1966 (2004).

665 25. H. Sano, A. D. Renault, R. Lehmann, Control of lateral migration and germ cell elimination
666 by the Drosophila melanogaster lipid phosphate phosphatases Wunen and Wunen 2. *J. Cell*
667 *Biol.* **171**, 675–683 (2005).

668 26. M. Slaidina, R. Lehmann, Quantitative Differences in a Single Maternal Factor Determine
669 Survival Probabilities among Drosophila Germ Cells. *Curr. Biol.* **27**, 291–297 (2017).

670 27. R. Warrior, Primordial Germ Cell Migration and the Assembly of the Drosophila
671 Embryonic Gonad. *Dev Biol* **166**, 180–194 (1994).

672 28. H. Oda, T. Uemura, Y. Harada, Y. Iwai, M. Takeichi, A *Drosophila* Homolog of Cadherin
673 Associated with Armadillo and Essential for Embryonic Cell-Cell Adhesion. *Dev. Biol.* **165**,
674 716–726 (1994).

675 29. U. Tepass, *et al.*, shotgun encodes Drosophila E-cadherin and is preferentially required
676 during cell rearrangement in the neurectoderm and other morphogenetically active epithelia.
677 *Genes Dev.* **10**, 672–685 (1996).

678 30. M. DeGennaro, *et al.*, Peroxiredoxin Stabilization of DE-Cadherin Promotes Primordial
679 Germ Cell Adhesion. *Dev. Cell* **20**, 233–243 (2011).

680 31. P. S. Kunwar, *et al.*, Tre1 GPCR initiates germ cell transepithelial migration by regulating
681 Drosophila melanogaster E-cadherin. *J. Cell Biol.* **183**, 157–168 (2008).

682 32. P. S. Kunwar, M. Starz-Gaiano, R. J. Bainton, U. Heberlein, R. Lehmann, Tre1, a G Protein-
683 Coupled Receptor, Directs Transepithelial Migration of Drosophila Germ Cells. *PLoS Biol.* **1**,
684 e80 (2003).

685 33. J. A. Campos-Ortega, V. Hartenstein, *The Embryonic Development of Drosophila melanogaster*
686 (Springer Science & Business Media, 2013).

687 34. D. Poulson, D. Waterhouse, Experimental Studies on Pole Cells and Midgut Differentiation
688 in Diptera. *Aust. J. Biol. Sci.* **13**, 541–567 (1960).

689 35. J. R. K. Seifert, R. Lehmann, Drosophila primordial germ cell migration requires epithelial
690 remodeling of the endoderm. *Development* **139**, 2101–2106 (2012).

691 36. G. Parés, S. Ricardo, FGF control of E-cadherin targeting in the Drosophila midgut impacts
692 on primordial germ cell motility. *J. Cell Sci.* **129**, 354–366 (2016).

693 37. D. Cai, *et al.*, Mechanical Feedback through E-Cadherin Promotes Direction Sensing during
694 Collective Cell Migration. *Cell* **157**, 1146–1159 (2014).

695 38. J. A. Glazier, F. Graner, Simulation of the differential adhesion driven rearrangement of
696 biological cells. *Phys. Rev. E* **47**, 2128–2154 (1993).

697 39. F. Graner, J. A. Glazier, Simulation of biological cell sorting using a two-dimensional
698 extended Potts model. *Phys. Rev. Lett.* **69**, 2013–2016 (1992).

699 40. P. Hogeweg, Evolving Mechanisms of Morphogenesis: on the Interplay between
700 Differential Adhesion and Cell Differentiation. *J. Theor. Biol.* **203**, 317–333 (2000).

701 41. D. Sweeton, S. Parks, M. Costa, E. Wieschaus, Gastrulation in Drosophila: the formation of
702 the ventral furrow and posterior midgut invaginations. *Development* **112**, 775–789 (1991).

703 42. B. Lin, J. Luo, R. Lehmann, An AMPK phosphoregulated RhoGEF feedback loop tunes
704 cortical flow–driven amoeboid migration in vivo. *Sci. Adv.* **8**, eabo0323 (2022).

705 43. M. Akhmanova, *et al.*, Cell division in tissues enables macrophage infiltration. *Science* **376**,
706 394–396 (2022).

707 44. M. K. Jaglarz, K. R. Howard, Primordial germ cell migration in Drosophila melanogaster is
708 controlled by somatic tissue. *Development* **120**, 83–89 (1994).

709 45. N. Metropolis, A. W. Rosenbluth, M. N. Rosenbluth, A. H. Teller, E. Teller, Equation of
710 State Calculations by Fast Computing Machines. *J. Chem Phys.* **21**, 1087–1092 (1953).

711 46. M. Starz-Gaiano, N. K. Cho, A. Forbes, R. Lehmann, Spatially restricted activity of a
712 Drosophila lipid phosphatase guides migrating germ cells. *Development* **128**, 983–991 (2001).

713 47. N. Zhang, J. Zhang, K. J. Purcell, Y. Cheng, K. Howard, The Drosophila protein Wunen
714 repels migrating germ cells. *Nature* **385**, 64–67 (1997).

715 48. A. H. Brand, N. Perrimon, Targeted gene expression as a means of altering cell fates and
716 generating dominant phenotypes. *Development* **118**, 401–415 (1993).

717 49. T. J. C. Harris, U. Tepass, Adherens junctions: from molecules to morphogenesis. *Nat. Rev.*
718 *Mol. Cell Biol.* **11**, 502–514 (2010).

719 50. S. Hong, R. B. Troyanovsky, S. M. Troyanovsky, Binding to F-actin guides cadherin cluster
720 assembly, stability, and movement. *J. Cell Biol.* **201**, 131–143 (2013).

721 51. R. B. Troyanovsky, E. P. Sokolov, S. M. Troyanovsky, Endocytosis of Cadherin from
722 Intracellular Junctions Is the Driving Force for Cadherin Adhesive Dimer Disassembly. *MBoC*
723 **17**, 3484–3493 (2006).

724 52. B.-A. Truong Quang, M. Mani, O. Markova, T. Lecuit, P.-F. Lenne, Principles of E-Cadherin
725 Supramolecular Organization In Vivo. *Curr. Biol.* **23**, 2197–2207 (2013).

726 53. Y. Wu, P. Kanchanawong, R. Zaidel-Bar, Actin-Delimited Adhesion-Independent
727 Clustering of E-Cadherin Forms the Nanoscale Building Blocks of Adherens Junctions. *Dev.*
728 *Cell* **32**, 139–154 (2015).

729 54. M. D. Martin-Bermudo, O. M. Dunin-Borkowski, N. H. Brown, Specificity of PS integrin
730 function during embryogenesis resides in the α subunit extracellular domain. *EMBO J.* **16**,
731 4184–4193 (1997).

732 55. A. Huttenlocher, Cell polarization mechanisms during directed cell migration. *Nat. Cell*
733 *Biol.* **7**, 336–337 (2005).

734 56. J. M. Halbleib, W. J. Nelson, Cadherins in development: cell adhesion, sorting, and tissue
735 morphogenesis. *Genes Dev.* **20**, 3199–3214 (2006).

736 57. M. Sandig, E. B. Voura, V. I. Kalnins, C.-H. Siu, Role of cadherins in the transendothelial
737 migration of melanoma cells in culture. *Cell Motil. Cytoskelet.* **38**, 351–364 (1997).

738 58. D. Vestweber, How leukocytes cross the vascular endothelium. *Nat. Rev. Immunol.* **15**, 692–
739 704 (2015).

740 59. Y.-T. Yeh, *et al.*, Three-dimensional forces exerted by leukocytes and vascular endothelial
741 cells dynamically facilitate diapedesis. *Proc. Natl. Acad. Sci.* **115**, 133–138 (2018).

742 60. J. Qi, N. Chen, J. Wang, C.-H. Siu, Transendothelial Migration of Melanoma Cells Involves
743 N-Cadherin-mediated Adhesion and Activation of the β-Catenin Signaling Pathway. *Mol. Biol.*
744 *Cell* **16**, 4386–4397 (2005).

745 61. C. E. Chan, D. J. Odde, Traction Dynamics of Filopodia on Compliant Substrates. *Science*
746 **322**, 1687–1691 (2008).

747 62. P. Maiuri, *et al.*, Actin Flows Mediate a Universal Coupling between Cell Speed and Cell
748 Persistence. *Cell* **161**, 374–386 (2015).

749 63. K. M. Yamada, M. Sixt, Mechanisms of 3D cell migration. *Nat. Rev. Mol. Cell Biol.* **20**, 738–
750 752 (2019).

751 64. V. Swaminathan, C. M. Waterman, The molecular clutch model for mechanotransduction
752 evolves. *Nat. Cell Biol.* **18**, 459–461 (2016).

753 65. L. B. Case, C. M. Waterman, Integration of actin dynamics and cell adhesion by a three-
754 dimensional, mechanosensitive molecular clutch. *Nat. Cell Biol.* **17**, 955–963 (2015).

755 66. L. J. Barton, L. R. la Cruz, R. Lehmann, B. Lin, The journey of a generation: advances and
756 promises in the study of primordial germ cell migration. *Development* **151**, dev201102 (2024).

757 67. D. J. Montell, P. Rorth, A. C. Spradling, slow border cells, a locus required for a
758 developmentally regulated cell migration during oogenesis, encodes Drosophila CEBP. *Cell* **71**,
759 51–62 (1992).

760 68. R. A. Foty, M. S. Steinberg, The differential adhesion hypothesis: a direct evaluation. *Dev.*
761 *Biol.* **278**, 255–263 (2005).

762 69. S. J. Gratz, *et al.*, Highly Specific and Efficient CRISPR/Cas9-Catalyzed Homology-Directed
763 Repair in Drosophila. *Genetics* **196**, 961–971 (2014).

764 70. W. F. Rothwell, W. Sullivan, Drosophila Embryo Collection. *Cold Spring Harb. Protoc.* **2007**,
765 pdb.prot4825 (2007).

766 71. J. Schindelin, *et al.*, Fiji: an open-source platform for biological-image analysis. *Nat. Methods*
767 **9**, 676–82 (2012).

768 72. M. H. Swat, *et al.*, Multi-Scale Modeling of Tissues Using CompuCell3D. *Methods Cell Biol.*
769 **110**, 325–366 (2012).

770

771

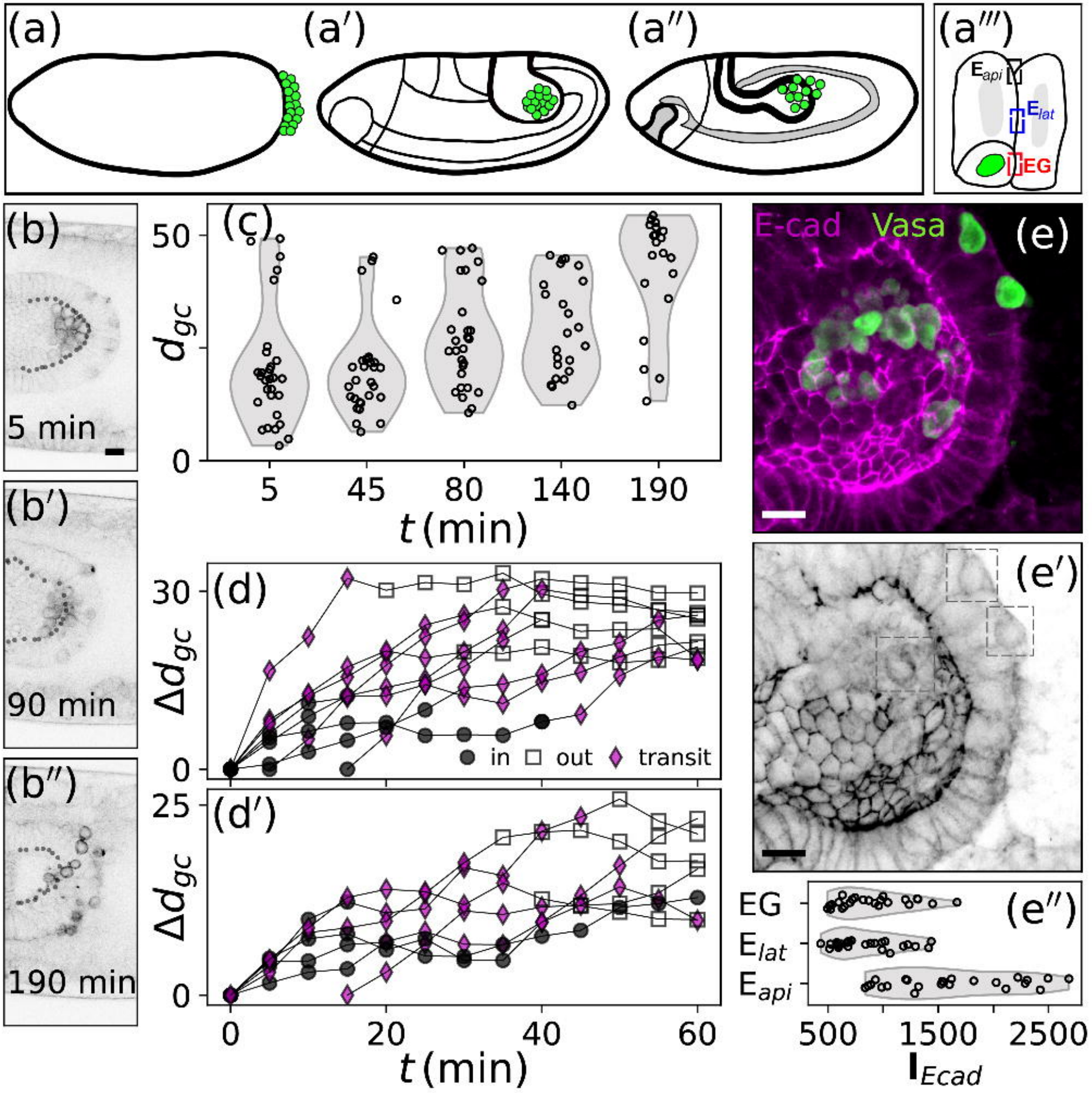
(a)
(a′)
(a″)
(a‴)
E_{api}
E_{lat}
EG
(b)
5 min
(b′)
90 min
(b″)
190 min
(c)
d_{gc}
50
0
5
45
80
140
190
t (min)
(d)
Δd_{gc}
30
0
in
out
transit
(d′)
Δd_{gc}
25
0
0
20
40
60
t (min)
E-cad
Vasa
(e)
(e′)
(e″)
EG
E_{lat}
E_{api}
500
1500
2500
I_{Ecad}

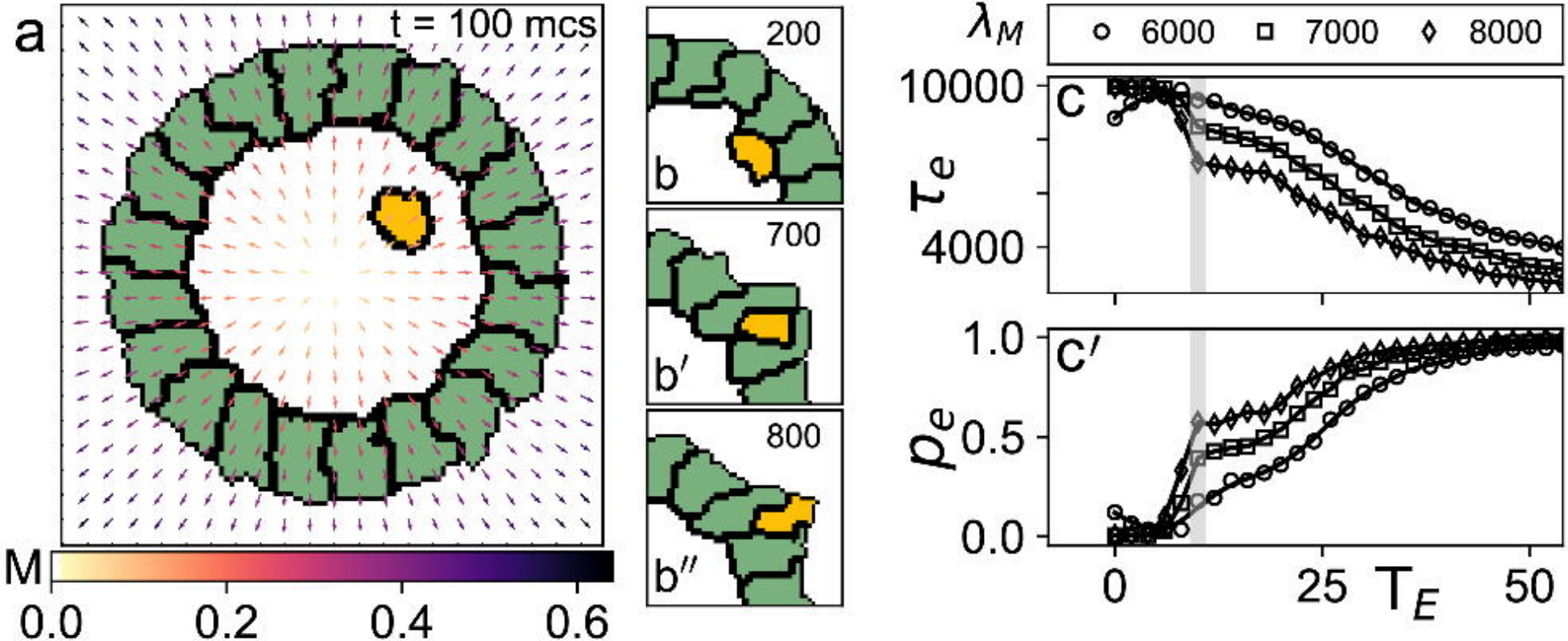
a
t = 100 mcs
M
0.0
0.2
0.4
0.6
200
b
700
b′
800
b″
λ_M
6000
7000
8000
10000
4000
c
τ_e
1.0
0.5
0.0
c′
ρ_e
0
25
50
T_E

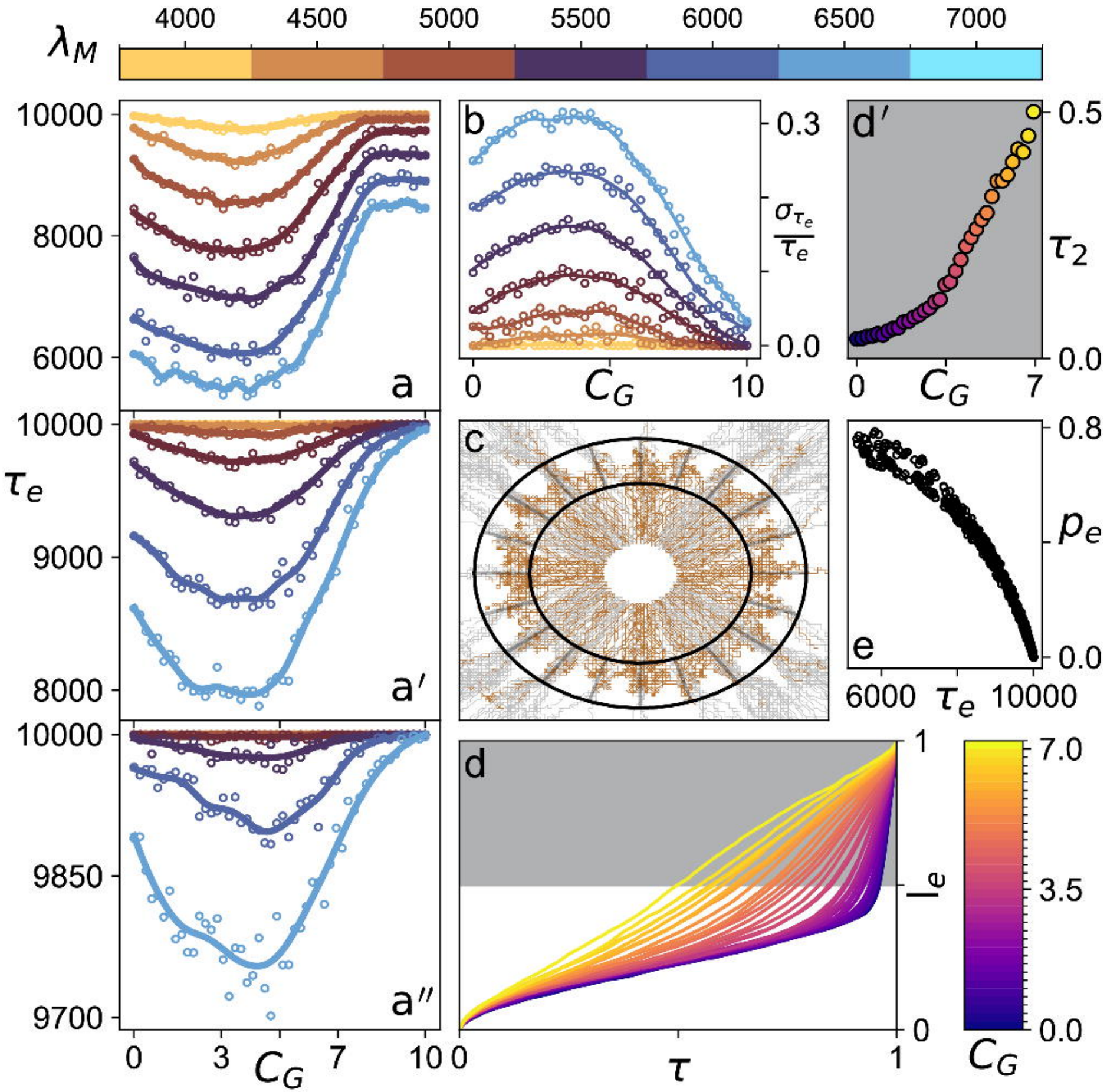
λ_M
4000
4500
5000
5500
6000
6500
7000
a
a′
a″
b
c
d
d′
e
τ_e
C_G
$\frac{\sigma_{\tau_e}}{\tau_e}$
τ_2
p_e
τ
Φ
10000
8000
6000
9000
9850
9700
0
3
7
10
0.3
0.0
0.5
0.8
1
7.0
3.5

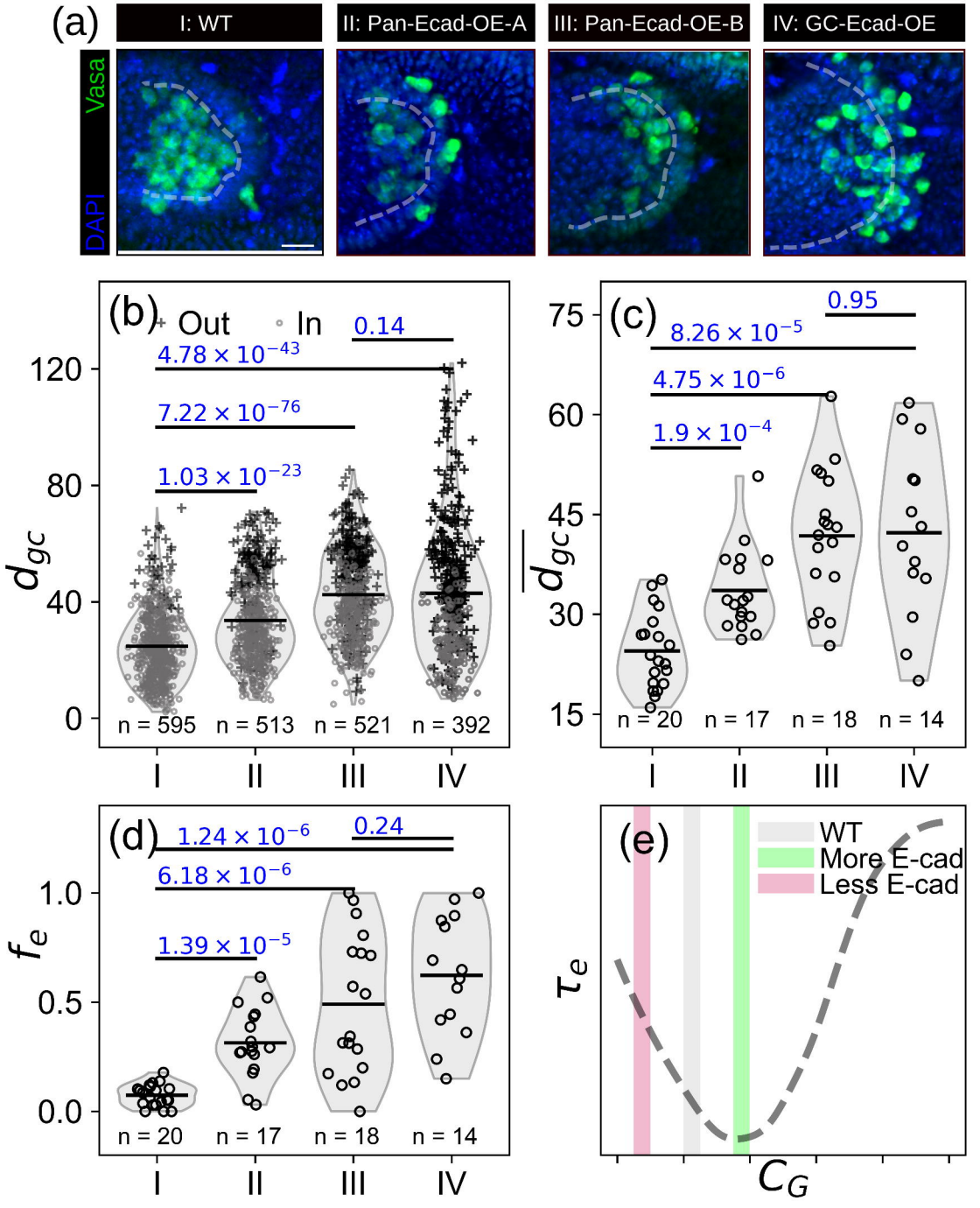
(a)
I: WT
II: Pan-Ecad-OE-A
III: Pan-Ecad-OE-B
IV: GC-Ecad-OE
Vasa
DAPI
(b)
Out
In
0.14
4.78 × 10^−43
7.22 × 10^−76
1.03 × 10^−23
d_gc
n = 595
n = 513
n = 521
n = 392
(c)
0.95
8.26 × 10^−5
4.75 × 10^−6
1.9 × 10^−4
n = 20
n = 17
n = 18
n = 14
(d)
1.24 × 10^−6
0.24
6.18 × 10^−6
1.39 × 10^−5
f_e
(e)
WT
More E-cad
Less E-cad
τ_e
C_G